Correcting biases in tropical cyclone intensities in low-resolution datasets using dynamical systems metrics

Davide Faranda, Gabriele Messori, Stella Bourdin, Mathieu Vrac, Soulivanh Thao, Jacopo Riboldi, Sebastien Fromang, Pascal Yiou

Correcting biases in tropical cyclone intensities in low-resolution datasets using dynamical systems metrics

Davide Faranda[1,2,3*], Gabriele Messori[4,5], Stella Bourdin[1], Mathieu Vrac[1], Soulivanh Thao[1], Jacopo Riboldi[4], Sébastien Fromang[1] and Pascal Yiou[1]

[1*]Laboratoire des Sciences du Climat et de l'Environnement, LSCE/IPSL, CEA-CNRS-UVSQ, Université Paris-Saclay, Gif-sur-Yvette, 91191, France.

[2]London Mathematical Laboratory, 8 Margravine Gardens London, W6 8RH, London, United Kingdom.

[3]LMD/IPSL, Ecole Normale Superieure, PSL research University, Paris, France.

[4]Department of Earth Sciences and Centre of Natural Hazards and Disaster Science (CNDS), Uppsala University, Uppsala, Sweden.

[5]Department of Meteorology and Bolin Centre for Climate Research, Stockholm University, Stockholm, Sweden.

*Corresponding author(s). E-mail(s): davide.faranda@lsce.ipsl.fr;
Contributing authors: gabriele.messori@geo.uu.se; stella.bourdin@lsce.ipsl.fr; mathieu.vrac@lsce.ipsl.fr; soulivanh.thao@lsce.ipsl.fr; jacopo.riboldi@geo.uu.se; sebastien.fromang@lsce.ipsl.fr; pascal.yiou@lsce.ipsl.fr;

Abstract

Although the life-cycle of tropical cyclones is relatively well understood, many of the underlying physical processes occur at scales below those resolved by global climate models (GCMs). Projecting future changes in tropical cyclone characteristics thus remains challenging. We propose a methodology, based on dynamical system metrics, to reconstruct the statistics of cyclone intensities in coarse-resolution datasets, where maximum wind speed and minimum sea-level pressure may not be accurately represented. We base our analysis on 411 tropical cyclones occurring between 2010 and 2020, using both ERA5 reanalysis data and observations from the HURDAT2 database, as well as a control simulation of the IPSL-CM6A-ATM-ICO-HR model. With ERA5 data, we compute two dynamical system metrics related to the number of degrees of freedom of the atmospheric flow and to the coupling between different atmospheric variables, namely the local dimension and the co-recurrence ratio. We then use HURDAT2 data to develop a univariate quantile–quantile bias correction conditioned on these two metrics, as well as a multivariate correction method. The conditional approach outperforms a conventional univariate correction of the sea-level pressure data only, pointing to the usefulness of the dynamical systems metrics in this context. We then show that the multivariate approach can be used to recover a realistic distribution of cyclone intensities from comparatively coarse-resolution model data.

Keywords: Tropical cyclones, Extreme Event, Bias Correction

1 Introduction

Tropical cyclones are among the most devastating natural disasters, often causing fatalities and extensive economic damage (Smith and Katz, 2013; Grinsted et al, 2019). They include several collateral hazards that can have significant impacts on people and property, such as rogue waves, flooding, extreme winds, and tornadoes. The few, most severe episodes account for the bulk of the costs associated with tropical cyclone (Emanuel, 2021). It is thus crucial to model such cyclones correctly. Unfortunately, even state-of-the-art global and regional climate models struggle to reproduce the dynamics of the most severe tropical cyclones (Camargo and Wing, 2016; Roberts et al, 2020b). This is mainly due to their insufficient resolution. Indeed, a grid spacing of the order of 10 kilometers or below is needed (Rotunno et al, 2009; Moon et al, 2020; Murakami et al, 2012; Manganello et al, 2012). Downscaling techniques can be employed to alleviate this issue, but their use is limited by computational costs; furthermore, different downscaling approaches can lead to diverging conclusions (e.g., Caron et al, 2011; Lee et al, 2020; Knutson et al, 2020; Emanuel, 2021). The situation is complicated by the reduced length of records in available tropical cyclone data sets, which mostly rely on satellite data not available before the '80s (Chang and Guo, 2007). This limitation hinders separating significant changes in tropical cyclone properties from decadal variability (Knutson et al, 2019).

Mid-latitude synoptic dynamics mostly originate from the chaotic structure of the motions associated with baroclinic instability (Lorenz, 1990; Schubert and Lucarini, 2015). Tropical cyclones are instead characterized by a rapid organization of unstable flows at the convective scale whose dynamics is turbulent and highly sensitive to boundary conditions (Muller and Romps, 2018;

Carstens and Wing, 2020). Here, we investigate whether it may be possible to exploit this high level of flow organization to obtain reliable statistics of intense tropical cyclones from relatively coarse-gridded atmospheric data. To achieve this, we compute two metrics that describe cyclones as states of a chaotic high-dimensional dynamical system. The first, the local dimension d, reflects the number of active degrees of freedom of an instantaneous state of the cyclone. The second, the co-recurrence ratio α, is a proxy for the instantaneous coupling between different atmospheric variables which may be interpreted in the sense of covariability. These metrics have recently provided insights on a number of geophysical phenomena, including transitions between transient metastable states (e.g. weather regimes) of the mid-latitude atmosphere (Faranda et al, 2017; Hochman et al, 2021a; Messori et al, 2021), drivers and predictability of extreme events (Messori et al, 2017; Hochman et al, 2019; De Luca et al, 2020; Faranda et al, 2020; Hochman et al, 2021b), palaeoclimate attractors (Brunetti et al, 2019; Messori and Faranda, 2021), slow earthquake dynamics (Gualandi et al, 2020) and changes in mid-latitude atmospheric predictability under global warming (Faranda et al, 2019). A benefit over previous dynamical systems approaches (e.g Wolf et al, 1985; Cao, 1997) is that these metrics can be easily applied to computationally demanding datasets, such as climate reanalyses or climate models.

Applications of d and α in the literature have used an Eulerian approach over a fixed spatio-temporal domain, rather than tracking the evolution of specific physical phenomena. Here, we follow the recent work of Faranda et al (2023) and apply the two metrics in a semi-Lagrangian perspective to characterize the structure of tropical cyclones in the $d - \alpha$ phase-space. That is, we compute the metrics on a spatial domain which follows the track of each cyclone in time. This enables the study of the complex behavior of convectively unstable flows, by focussing on the evolution of the storm's structure instead of the storm's motion across a fixed domain (Crisanti et al, 1991; Vulpiani, 2010). The signature of intense cyclones is associated with the presence of inverse energy cascades as suggested by Levich and Tzvetkov (1985) and, more recently, by Faranda et al (2018); Dunkerton et al (2009); Tang et al (2015). Such inverse cascades are associated with potential–kinetic energy conversions and are particularly notable for intense storms (Bhalachandran et al, 2020). These energy conversions are related to the deep convection in the eyewall, that redistributes to the upper troposphere the enthalpy gained thanks to surface heat fluxes in the boundary layer. Such local processes contribute to the generation of the storms' warm core and, ultimately, to wind intensification at the larger, sub-synoptic scale of the storm (Emanuel, 1986). We hypothesise that these exchanges have a signature in both the large-scale horizontal velocity and potential vorticity fields, which are reasonably well-represented in coarse simulations or reanalyses. If this indeed holds, then the dynamical system metrics should be able to distinguish between different storm intensities due to their different degree of organization and coupling. This would enable a correction conditioned on d and α of cyclone intensity statistics in datasets where we cannot explicitly access the spatial scales underlying the dynamics of intense tropical cyclones.

Bias correction of climate models is a crucial step in improving the accuracy of climate predictions, and there is a considerable number of different bias correction techniques proposed in the literature. For a review of bias correction methodologies, which is beyond the purpose of this paper, we refer the reader to Maraun (2016). One widely used method is empirical Quantile mapping bias correction (QMBC), which has been shown to be effective in reducing biases in precipitation and temperature data (e.g., Li et al (2010); Michelangeli et al (2009); Cannon et al (2015); Cannon (2018)). QMBC has also been applied to assessing the impact of climate change on tropical cyclone (TC) intensity in medium-resolution global climate models (GCMs)(Zhao and Held, 2010; Sugi et al, 2017; Yoshida et al, 2017). These studies have shown that QMBC is very useful in improving the accuracy of GCM simulations by matching the distribution of observed data with the model's output. However, the conventional QMBC has limitations, including not accounting for non-stationary characteristics of the data. In this study, we propose a new method for bias correction that implicitly accounts for weak non-stationarity in the data through the dynamical systems metrics, and that may be easily extended to explicitly account for non-stationarity by leveraging well-tested approaches. We demonstrate its effectiveness in improving the accuracy of TC intensity projections.

We base our analysis on best track cyclone data from the HURDAT2 database, which we take as ground truth, ERA5 reanalysis data and a high-resolution global climate model simulation. We compute the two dynamical systems metrics using the square root of the kinetic energy uv [m/s] and the potential vorticity field PV [PVU] at the 850 hPa level. The rationale for using PV follows the works of Peng et al (2012) and Fu et al (2012) who used PV for distinguishing developing versus non-developing disturbances. The square root of the horizontal kinetic energy uv is relevant to the study of tropical cyclones because of its direct connection with the wind speed and with the phases of rapid intensification/decay of the cyclones (Krishnamurti et al, 2005). The 850 hPa level is chosen because it lies in-between the planetary boundary layer and the middle troposphere, where most of the potential–kinetic energy conversions occur in tropical cyclones (Camargo et al, 2007). Although some of the information provided by PV and uv is redundant, they are analytically connected, and thus we find that their coupling provides nontrivial information which justifies their use.

Our study is organized as follows: first, we describe the data, variables for cyclone dynamics and the theoretical bases supporting the computation of the dynamical system metrics. Then, we show the general characteristics of the phase space of tropical cyclones in reanalysis data for the different variables, and use these to define a quantile–quantile correction approach for cyclone intensities conditioned on the two dynamical systems metrics. The correction is performed on ERA5 reanalysis, using sea-level pressure (SLP) from HURDAT2 as ground truth. We then conduct an out-of-sample test comparing this approach to an unconditional quantile–quantile correction. Finally, we test this correction on data from a GCM.

2 Data

2.1 HURDAT2 tropical cyclone data

We follow 197 North Atlantic and 214 eastern North Pacific tropical cyclones that occurred between 2010 and 2020, using the HURDAT2 Best Track Data (Landsea and Franklin, 2013). We use six-hourly information on the location and central pressure of the cyclones, as well as their time of landfall or special intensity report points.

2.2 Representation of tropical cyclones in ERA5 data

We base our analysis on instantaneous[1] $uv = u^2 + v^2$, SLP and PV at 850hPa from the ERA5 reanalysis (Hersbach et al, 2020), sampled every 6h and additionally whenever the HURDAT2 database displays a cyclone landfall entry or special intensity report points. The horizontal resolution of the data is 0.25°. We also make use of ERA5 data coarse-gridded to a 0.5° horizontal resolution using a nearest neighbour approach. In the vast majority of cases, the SLP difference in the four ERA5 gridpoints around the cyclone core is 1 hPa or less. Using a nearest neighbour approach thus provides similar results to other coarse-graining approaches. The coarse-grained dataset will be hereinafter referred to as ERA5 cg, and will be used to evaluate the sensitivity of our conclusions to the resolution of the dataset. When comparing ERA5 to HURDAT2, we verify that the SLP minimum in ERA5 is located within a region of 5° of the HURDAT2 cyclone position. For our analysis we do not use the wind data because this quantity is often used in different ways (e.g. sustained winds vs. wind-gusts and with different averaging times) to assess TC intensity in reanalyses, models and the HURDAT2 database, while the use of minimum SLP is coherent across all datasets.

There is often a large discrepancy between the minimum SLP reported in HURDAT2 and that in ERA5 (Fig. 1a,c). Especially for the most intense cyclones, ERA5 systematically underestimates minimum SLP. The biases are larger in the eastern North Pacific than in the North Atlantic basin (cf. Fig. 1a and 1c). This affects the capability of ERA5 to accurately assign each tropical cyclone to the appropriate Saffir-Simpson category (Simpson and Saffir, 1974), which we here use relative to SLP (see Table 1). Indeed, recent research argues that SLP is more closely related to cyclone damage than maximum sustained winds (Klotzbach et al, 2020). In particular, ERA5 has a negative bias in the number of tropical cyclones stronger than category 2, namely min(SLP)<980 hPa. While this bias is present in both the North Atlantic and eastern North

[1] We follow here ECMWF's terminology, see: https://confluence.ecmwf.int

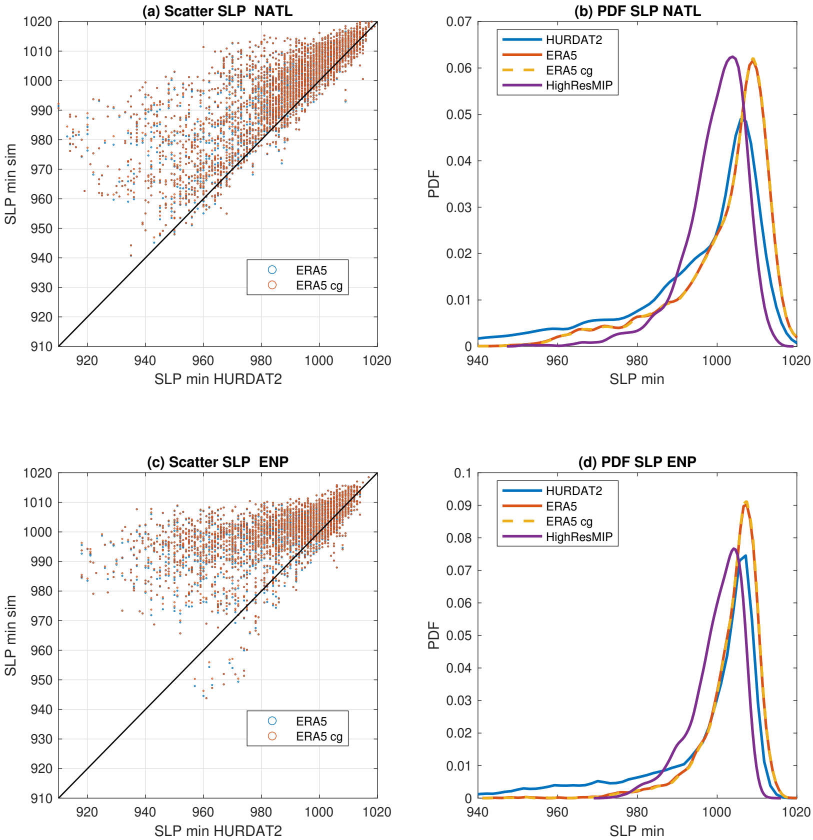

Fig. 1 Scatterplot of minimum SLP for (a) North Atlantic [NATL] and (c) eastern North Pacific [ENP] tropical cyclones in HURDAT2 versus ERA5 and ERA5 cg. Probability density functions of minimum SLP for (b) North Atlantic and (d) eastern North Pacific tropical cyclones in HURDAT2, ERA5, ERA5 cg and the IPSL-CM6A-ATM-ICO-HR model.

Pacific basins, in the latter the biases for the most intense cyclones appear more severe. This might be due to the more intermittent aircraft reconnaissance activity in that basin with respect to the North Atlantic (Knaff et al, 2021). The coarse-graining operation does not notably affect the distribution of cyclone SLP minima (Fig. 1b, d), likely because of the above-mentioned weak SLP variations in the ERA5 dataset in the gridboxes immediately surrounding the cyclone core. We underline that the two ERA5 horizontal resolutions used here are of the same order of magnitude as those of the HighResMIP (High Resolution Model Intercomparison Project, Haarsma et al, 2016) and PRIMAVERA models, which are amongst the current best tools to study climate change impacts on tropical cyclones (Roberts et al, 2020a).

2.3 Representation of tropical cyclones in IPSL-CM6A-ATM-ICO-HR model data

For the purpose of this study, we used a simulation performed with the IPSL-CM6A model (Boucher et al, 2020). Model configuration is atmosphere-only (ATM) with forced sea-surface temperatures (SST). The physics component of the model is LMDZ6A, as described in Hourdin et al (2020). The dynamical core is Dynamico (Dubos et al, 2015, ICO,), which uses an icosahedral grid. A run at high-resolution (HR) is used, corresponding to 0.5° horizontal resolution. The CM6A version of the IPSL model has 79 vertical levels. The configuration is named IPSL-CM6A-ATM-ICO-HR. The run was perfomed for the HighResMIP, therefore following the protocol described in (Haarsma et al, 2016). It is a historical run, over the 1950-2014 period (65 years). Greenhouse gases, aerosols and SSTs are forced to the observed values.

We use the TC tracking algorithm from Ullrich et al (2021). We additionally remove tracks starting at latitudes above 30° to minimise incorrect classification of extratropical lows as tropical systems.

The model produces a total of 327 tropical cyclones in the North Atlantic and 989 in the eastern North Pacific (defined following Knutson et al, 2020). Among them, 150 are randomly sampled for each basin, which is deemed a sufficiently large statistical sample for our analysis. The total number of cyclones reproduced by the IPSL-CM6A-ATM-ICO-HR model is in line with that of other HighResMIP models with similar resolution (cf. Roberts et al, 2020b).

A comparison of the distribution of HURDAT2 SLPs with those in the model and in the ERA5 and ERA5 cg data (Fig. 1b, d), suggests that current state-of-the-art GCMs and ERA5 both encounter difficulties when it comes to representing the intensity of tropical cyclones (Kim et al, 2018). Specifically, all three datasets have a sparsely populated left tail of the minimum SLP distribution and, especially for the North Atlantic basin, a different mode when compared to HURDAT2.

3 A dynamical systems view of tropical cyclones

In our analysis, for every cyclone we adopt 6-hourly domains of approximately 1200 km × 1200 km at latitudes 10 °N–25 °N (41 × 41 grid points in ERA5 corresponding to 10° latitude ×10° longitude), centred at every timestep on the HURDAT2 cyclone location for ERA5 and centered on the minimum of sea-level pressure for the model simulation. We then consider PV and uv at 850 hPa in this domain. Each instantaneous state of the cyclone, as represented by these variables and domains, corresponds to a point along a phase-space trajectory representing the cyclone's evolution. We sample this trajectory at discrete intervals determined by the temporal resolution of our data. Our aim is to diagnose the dynamical properties of the instantaneous (in time) and local (in phase-space) states of the cyclone (physical space in Fig. 2). To do so, we leverage two metrics issuing from the combination of extreme value theory with Poincaré recurrences (Freitas et al, 2010; Lucarini et al, 2012,

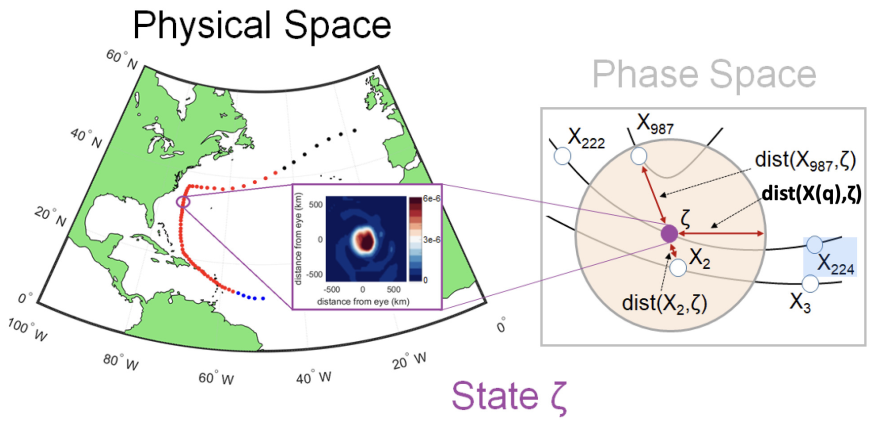

Fig. 2 Schematic of the computation of the dynamical systems metrics for an instantaneous state of a tropical cyclone. We take a snapshot of the cyclone in physical space (black quadrant), PV in this example, which corresponds to state ζ in our phase space. The shaded circle is a 2D representation of the surface determined by the high threshold $s(q, \zeta)$, which defines recurrences of ζ. The distances between measurements defined by $\mathrm{dist}(X_i, \zeta)$ are marked by double-headed arrows. For all points within the hyper-sphere, $\mathrm{dist}(X_i, \zeta) < s(q, \zeta)$ and $g(X_i, \zeta) > s(q, \zeta)$ hold. Here, i represents the timestep in the dataset. In the schematic, only two measurements qualify as recurrences: timesteps 2 and 987 (adapted from Messori and Faranda (2021)).

2016). Recurrences are temporally separated PV or uv states that resemble each other. As we discuss below, identifying these recurrences is instrumental to compute the two dynamical systems metrics.

We first calculate TC-centered maps of PV and uv to define the TC state i, where $i = 0, 1, ..., T-1, T$ represents a given timestep in our dataset, T being the total number of timesteps. We then normalize each distance by their respective norms, which yields PV_i and uv_i, respectively. Finally, we define the TC state at a given timestep, X_i, as the pair of PV_i and uv_i maps at that timestep. We thus construct a semi-Lagrangian framework tracking each cyclone. We take each pair of maps X_i in turn as the reference state ζ in our calculation (phase space in Fig. 2). We then define logarithmic returns as:

$$g(X_i, \zeta) = -\log[\mathrm{dist}(X_i, \zeta)] \tag{1}$$

Here, we define dist as the Euclidean distance between pairs of maps, but it can be chosen as any distance metric between two vectors. In principle, ζ can be any state (and does not have to belong in the available X_i). In practice, ζ is one of the X_i, and the $\log \mathrm{dist}$ is computed for all other time steps, as $\log(\mathrm{dist}(X, X))$ is not defined. Note that the distances between maps are computed by respecting the order of the grid points but without specifying their actual position on the maps (longitude and/or latitude). The logarithmic weight comes directly from the Poincaré recurrence theorem, which states that the probability of hitting a ball centered on a state in phase space gets exponentially small when linearly reducing the radius of the ball. Since dist tends to zero as pairs of X_is increasingly resemble each other, the series of logarithmic returns g_i takes large values for X_i closely resembling ζ. The minus sign in Eq. 1 has the function to convert the minima of the distances into the maxima of g, as it is common practice in extreme value theory to define extreme value distributions for maxima rather than for minima. In Fig. 2, an example of the phase space and the geometrical object defined above is provided: the shaded circle is a 2D representation of the surface (in general this is a hyper-sphere for higher dimension) determined by the high threshold $s(q,\zeta) = g(X(q),\zeta)$, which defines recurrences of ζ. The distances between measurements are marked by double-headed arrows. For all points within the hyper-sphere, $\mathrm{dist}(X_i,\zeta) < \mathrm{dist}(X(q),\zeta)$ and $g(X_i,\zeta) > s(q,\zeta)$ hold.

We next define exceedances as $u(g,\zeta) = \Pr(g \mid g(X_i,\zeta) > s(q,\zeta))$, where $s(q,\zeta)$ is a high threshold corresponding to the quantile q of $g(X_i,\zeta)$. These are effectively the previously-mentioned Poincaré recurrences, for the chosen state ζ (phase space in Fig. 2). The Freitas-Freitas-Todd theorem (Freitas et al, 2010; Lucarini et al, 2012) states that the cumulative probability distribution $u(\zeta) = F(g,\zeta)$ can be approximated by the exponential member of the Generalised Pareto Distribution (i.e. with shape and location parameters equal to zero). We thus have that:

$$u(g,\zeta) = F(g,\zeta) \simeq \exp\left[-\frac{g(\zeta)}{\sigma(\zeta)}\right] \tag{2}$$

The parameters u and σ, the scale parameter of the Generalized Pareto Distribution, depend on the chosen state ζ. From the above, we can define the local dimension d as: $d(\zeta) = 1/\sigma(\zeta)$, with $0 < d < +\infty$. The Freitas-Freitas-Todd theorem thus enables us to estimate numerically d from a series of uv or PV data over the semi-Lagrangian domain based on their Poincaré recurrences. The numerical procedure is rather simple: i) we fix $\zeta = X_i$ for a given time step i, ii) we fix s to be the threshold corresponding to the quantile $q = 0.98$. iii) we obtain all the $u(\zeta)$, namely the 2% (because $q = 0.98$) of maps having the smallest euclidean distances from ζ, iv) we use the fact that Eq.2 is an exponential to estimate σ, its standard deviation, as the average value of u once we subtract s. Here we are just using the fact that in the exponential function, average and standard deviation are equal.

Next, we introduce logarithmic returns and high thresholds separately for PV and uv as $g(PV_i)$, $s_{PV}(q)$ and $g(uv_i)$, $s_{uv}(q)$ respectively. These allow us to investigate the way in which PV and uv co-vary by defining the co-recurrence ratio α:

$$\alpha(\zeta) = \frac{\nu[g(PV_i) > s_{PV}(q) \mid g(uv_i) > s_{uv}(q)]}{\nu[g(PV_i) > s_{PV}(q)]} \tag{3}$$

with $0 \leq \alpha \leq 1$. Here, $\nu[-]$ is the number of events satisfying condition $[-]$, and all other variables are defined as before. In practice, if all PV recurrences match a uv recurrence, then the number of conditional PV events (numerator) is the same as the number of unconditional PV events (denominator) and hence $\alpha = 1$. In contrast, if PV recurrences never match uv recurrences, then the numerator is zero and hence $\alpha = 0$. By definition, α is symmetric with respect to the choice of variable (PV or uv), since $\nu[g(PV_i) > s_{PV}(q)] \equiv \nu[g(uv_i) > s_{uv}(q)]$. In other words, the number of events above a given quantile is the same for either variable, given that they are both taken from the same set of TC snapshots. The section "Code availability" provides information on how to download the package used to compute d and α.

While the derivation of d and α may seem very abstract, the two metrics can be related intuitively to the physical properties of the tropical cyclones. d is a proxy for the active number of degrees of freedom of the cyclones' instantaneous states, while α measures the coupling between different variables. The relationship between dynamical systems metrics and the structure of tropical cyclones is elucidated in Figure 3. d and α are anti-correlated: low dimensionality is generally associated to a high coupling between the PV and uv maps, while the opposite holds for high dimensionality (Fig. 3a). Most of the considered time steps fall in a regime of relatively low dimensionality relative to the number of gridpoints in the lagrangian domain (41^2), and of low coupling. We first investigate the uv and PV atmospheric patterns corresponding to these timesteps. To do so, we consider all points below the 0.95 quantiles of the d and α distributions, corresponding to thresholds of d_H=30 and α_H=0.35. These data show a clear, albeit relatively weak, cyclonic structure in PV, with values peaking at $\sim$2 PVU (Fig. 3b). The uv pattern also reflects a cyclonic structure, with values peaking at $\sim$ 12 m s^{-1} (Fig. 3e). The picture is radically different for cyclone timesteps with $d > d_H$ or $\alpha > \alpha_H$ (Fig. 3c,d,f,g). High values of d feature a smaller, weaker PV core than the bulk of the data, which is reflected in low values of the square root of the kinetic energy (Fig. 3c,f). High values of α instead correspond to an intense cyclonic PV core and a correspondingly high uv around it (Figs. 3d,g). The same qualitative features emerge also for the ERA5 cg and HighResMIP data (not shown). To illustrate this for single cyclones, Fig. 4 shows an example of two snapshots: one with very high α and low d and one with very low α and high d. These two examples confirm the conclusion drawn from the composite means, altough we cannot directly compare the results presented in Figs. 3-,4 because the first is about composite averages while the second about single cases.

These results reflect the high degree of symmetry and organization found in intense tropical cyclones with respect to weaker disturbances (e.g., Emanuel, 1986, 1997; Montgomery and Smith, 2017). Intense tropical cyclones display a quasi-axisymmetric shape: a state where very few degrees of freedom (i.e., low d values, which typically correspond to high α values) are needed to describe their dynamics because of the air parcels all aligning with the cyclones' circulation. On the contrary, the cyclones with higher dimensionality likely display asymmetric or multiple PV patches (as for the example shown in Fig. 4b), with a less organised kinetic energy landscape. This variable geometry of the PV pattern may explain the different degrees of coupling between uv and PV.

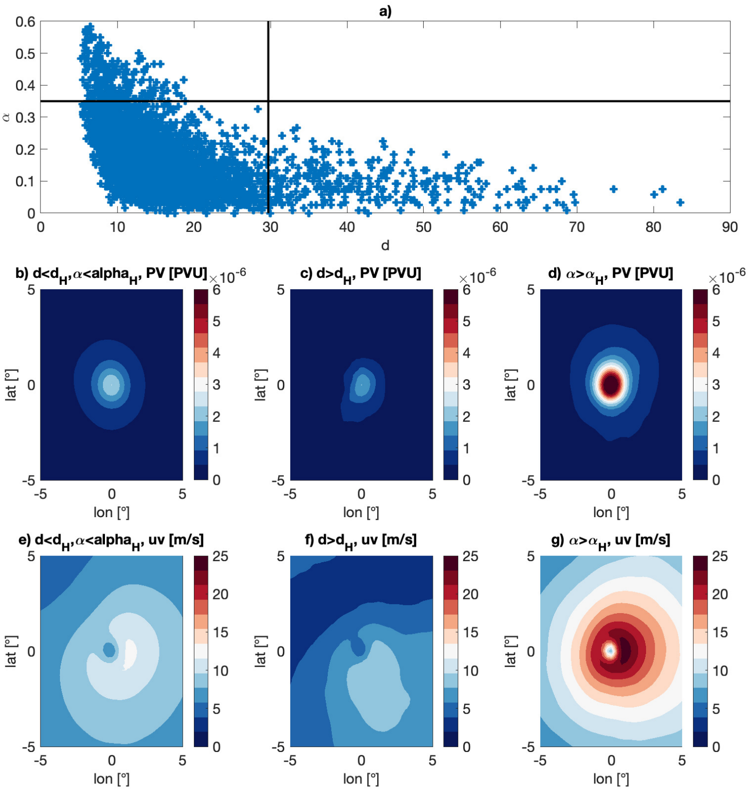

Fig. 3 The scatter plot displays the values of the local dimension d and the co-recurrence α computed on ERA5 uv and PV maps during tropical cyclone timesteps in the NATL basin. The vertical and horizontal black solid lines mark the 0.95 quantiles of the d and α distributions, namely d_H and α_H, respectively. The maps show composites of PV (b–d) and uv (e–g) for $d < d_H, \alpha < \alpha_H$ (b,e), $d > d_H$ (c,f) and $\alpha > \alpha_H$(d,g).

The connection between d, α and cyclone intensity broadly holds when diagnosing the intensity of the cyclones using the minimum SLP, computed from gridded data (Fig. 5). In general, large values of α (colorscale) correspond to low values of the minimum SLP in both the North Atlantic and eastern North Pacific basins. Moreover, the most intense tropical cyclones phases are marked by a low dimension d. Similar conclusions hold for the HighResMIP data, as further discussed in Sect. 4b. Remarkably, the coarse-graining operation on ERA5 data does not alter sensibly the dynamical properties d and α, and the two metrics maintain roughly the same range of values as in the original 0.25° reanalysis (Fig. 5b, d). The explanation for this stability follows that given in Faranda et al (2017) for the SLP data over the North Atlantic:

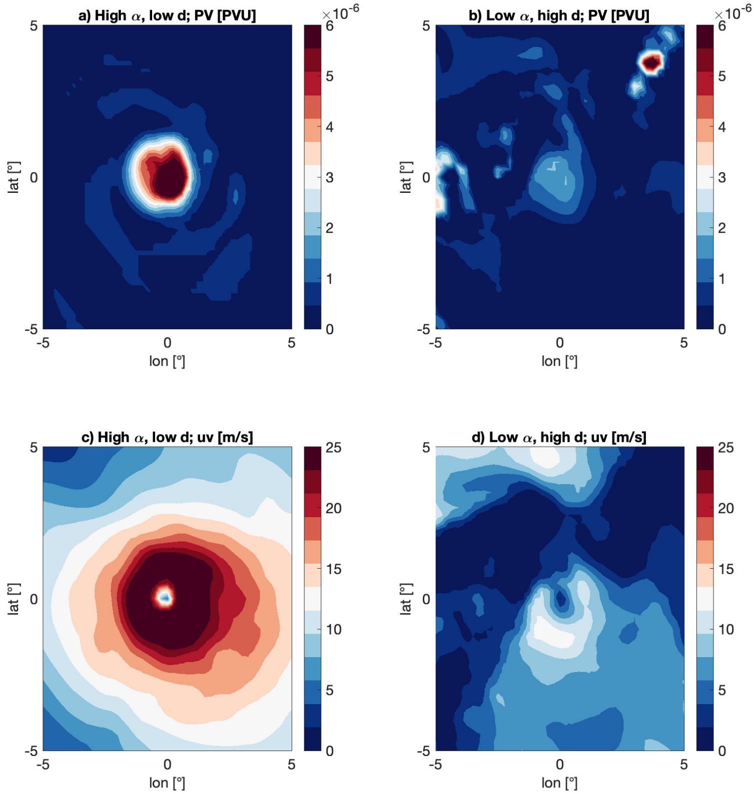

Fig. 4 As Fig. 3b–g, but for an example of a single cyclone snapshot with $\alpha = 0.61$ and $d = 6.02$ (a,c) and $\alpha = 0.08$ and $d = 12.36$ (b,d).

the dynamical systems metrics are practically insensitive to resolution, provided that the resolution is sufficient to represent the underlying dynamics of the data. This is the case here since, as previously discussed, ERA5 cg and ERA5 share near-identical distributions of cyclone SLP minima.

4 Bias Corrections of tropical cyclone sea-level pressure minima

4.1 Bias Corrections of ERA5 tropical cyclone sea-level pressure minima

We perform two bias corrections for ERA5 minimum sea-level pressure. In both cases we prepare our data as follows. Firstly, we rearrange our set of

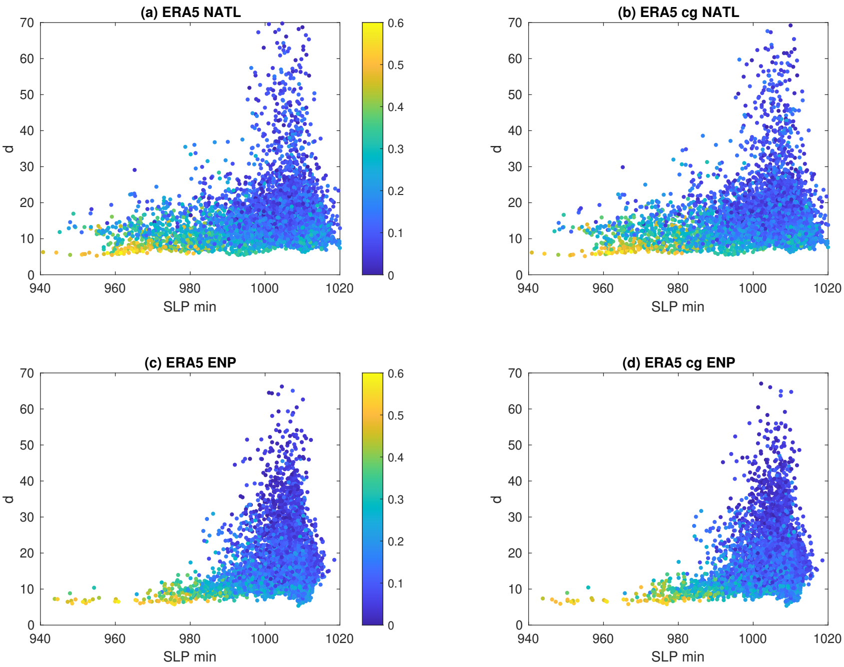

Fig. 5 Scatterplots of minimum SLP vs local dimension d and co-recurrence ratio α (colorscale) calculated on uv and PV at 850 hPa for (a,c) ERA5 and (b,d) ERA5 cg, in the (a,b) North Atlantic [NATL] and (c,d) eastern North Pacific [ENP] basins.

tropical cyclones randomly. This mixes tropical cyclones from different years and different parts of the cyclone season in the training and in the verification datasets. We thus avoid intraseasonal effects and possible non-stationarities linked to anthropogenic climate change or interannual variability of the atmospheric circulation. We then consider the first 4000 datapoints of our rearranged HURDAT2 SLP minima for each basin as training data and the remaining 2029 datapoints for the North Atlantic basin and 2313 datapoints for the eastern North Pacific basin as verification data. This same split is also applied to ERA5 cg.

We next define objective metrics to determine whether our bias corrections improve the cyclone intensities. We use the original Simpson and Saffir (1974) scale of tropical cyclones classification based on the SLP minima and define cyclone categories for the verification datasets (Table 1). We define two error metrics: the total count of tropical cyclones time-steps with the wrong category Err_T, and the count of major tropical cyclones (intensity$\geq$3) with wrong category Err_C.

The first bias correction we implement is an unconditional quantile-quantile correction. We begin by subtracting the median of the distributions of SLP minima from the data, which we then add back at the end of the procedure. We then compute the difference Δq between the empirical cumulative density functions (ECDFs) of SLP minima in HURDAT2 with respect to ERA5 and ERA5 cg evaluated at 100 quantile values q. For each data to correct, the closest quantile $q*$ in the ECDF(ERA5) or ECDF(ERA5 cg) dataset is found and the value $\Delta q*$ is added to the original value.

The second bias correction approach is conditioned on the dynamical systems metrics. The results presented in Figures 3 and 5 show that we can discriminate intense tropical cyclones as those having a large value of α and a small value of d. We test several d_H and α_H pairs (using the same convention of Fig.3) to separate the training dataset into intense ($d < d_H$, $\alpha > \alpha_H$) and non-intense cyclones. We next apply the previously described quantile-quantile correction to the two subsets of cyclones separately. We then use a grid-search approach and scan all combinations of $10 \leq d \leq 38$ and $0.1 \leq \alpha \leq 0.34$, with resolution $\Delta d = 1$ and $\Delta\alpha = 0.1$, to find the values d_c and α_c that minimise the total error

$$Err = Err_T(ATL) + Err_T(ENP) + Err_C(ATL) + Err_C(ENP). \qquad (4)$$

We additionally impose that the chosen values improve upon the unconditional correction for both basins and both Err_T and Err_C. By randomizing cyclone timesteps, we obtain two different sets of 100 realizations for ERA5 and ERA5 cg training datasets, respectively, which allow to compute two distributions each containing 100 values of d_c and α_c. The boxplots of such distributions are presented in Fig.6. We then select the median over each sample. This analysis yields $d_c = 21$ and $\alpha_c = 0.16$ for ERA5 and $d_c = 19$, $\alpha_c = 0.165$ for ERA5 cg. The standard deviations of d_c and α_c are respectively 4 and 0.04. We can deduce that the minimisation has some sensitivity to the choice of samples. We will refer to these parameters as the best set that realizes the bias correction for the data presented in this study.

We illustrate in detail the improvement obtained with the two bias correction approaches in Figures 7-8. Panels (a,b) show that the ECDFs of bias-corrected SLPs are closer to the verification dataset HURDAT2 than the non-corrected ones. However, panels (c,d) show that the correspondence of observed versus modelled SLPs for individual cyclones is not necessarily improved by the bias correction. Specifically, for some of the tropical cyclone timesteps, the bias correction attributes a higher category than the original data. This is shown in panels (e,f) in terms of Δ between the categories as estimated for ERA5 (cg) data relative to HURDAT2. Finally panels (g,h) show the evident improvements in terms of intensity histograms: the original non corrected data virtually have no category 4 or 5 tropical cyclones, whereas with the corrections we are able to retrieve the full cyclone intensity spectrum. The difference between ERA5 and ERA5 cg is limited, although a comparison of panels (d,h) between Figs. 7 and 8 evidences that the coarse-graining does have some effect on the most intense cyclones. As previously noted, a clear difference emerges between the NATL and ENP basins, with the latter generally showing larger

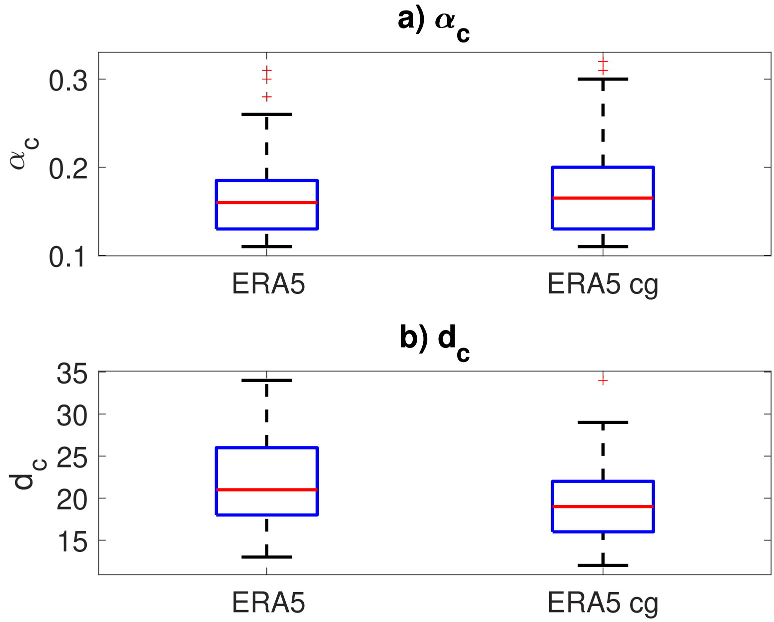

Fig. 6 Boxplots for 100 realizations of the grid search procedure used to estimate the values of α_c and d_c which minimize the total error in Eq. 4 . On each box, the central mark indicates the median, and the bottom and top edges of the box indicate the 25th and 75th percentiles, respectively.

biases for both the uncorrected and corrected data. The difference between the conditional and unconditional bias corrections also emerges chiefly in the ENP. Indeed, the two perform comparably in the NATL, while in ERA5 and especially in ERA5 cg, the conditional correction shows a vastly improved performance.

Category	wind [m/s]	minimum sea-level pressure [hPa]
1	33–42	$\geq$980
2	43–49	965–979
3	50–58	945–964
4	59–69	920–944
5	>69	$\leq$920

Table 1 Saffir-Simpson tropical cyclone intensity classification.

4.2 Bias Corrections of HighResMip tropical cyclone sea-level pressure minima

When looking at the cyclone SLP minima for the HighResMIP data, we remark immediately the virtual lack of minima below 960 hPa and the reduced range

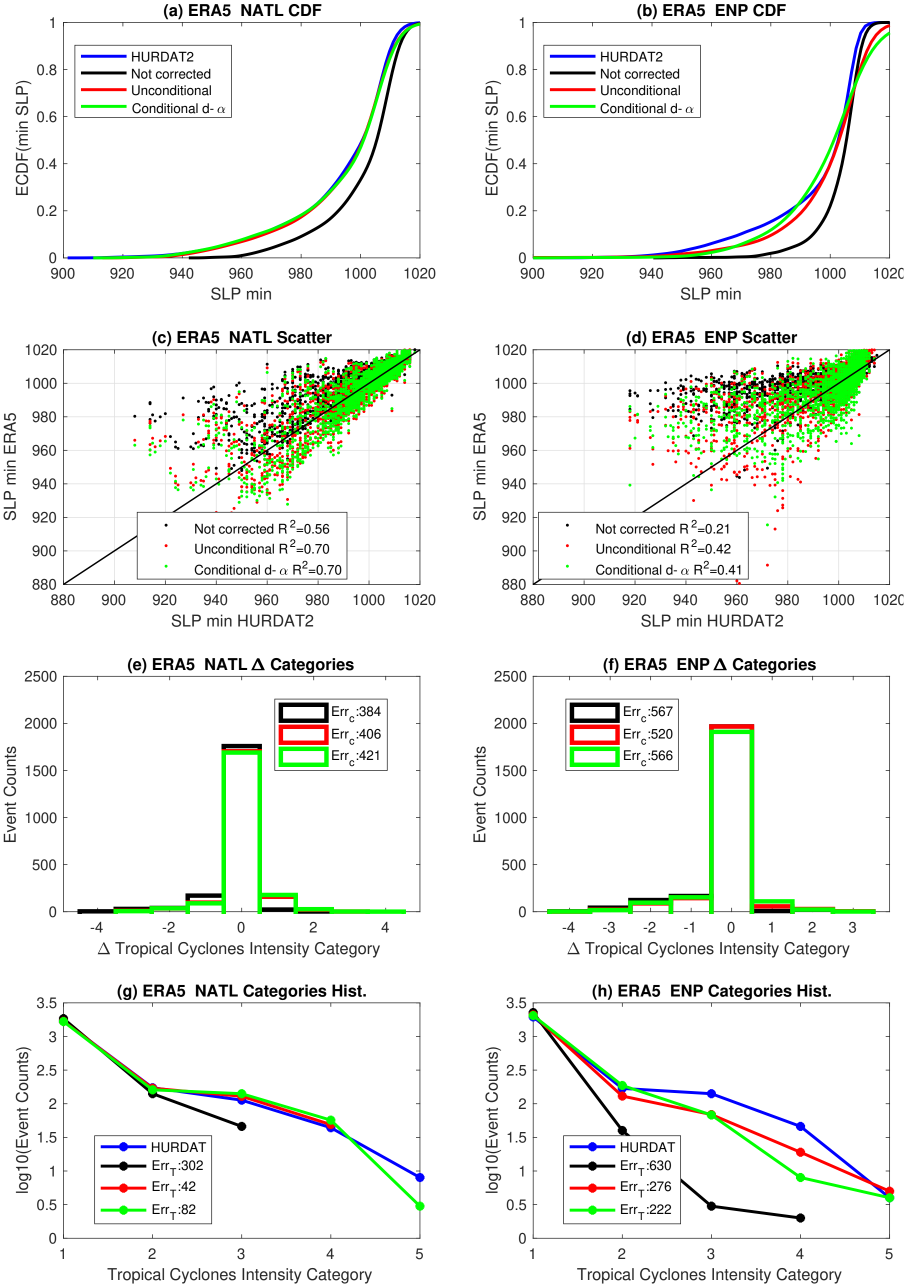

Fig. 7 Unconditional bias correction and bias correction conditioned on the dynamical systems metrics for the best d and α parameters combination (see Fig. 6, $\alpha_c = 0.16$, $d_c = 21$) for a realization of the ERA5 data sample. (a,b) Empirical cumulative density functions (ECDFs), (c,d) scatter plots, (e,f) error Err_c in category intensities (negative values imply underestimation, positive values overestimation), (g,h) histogram of category intensities and ERR_T in the inset. (a,c,e,g) North Atlantic [NATL], (b,d,f,h) eastern North Pacific [ENP] basins. See legends for details.

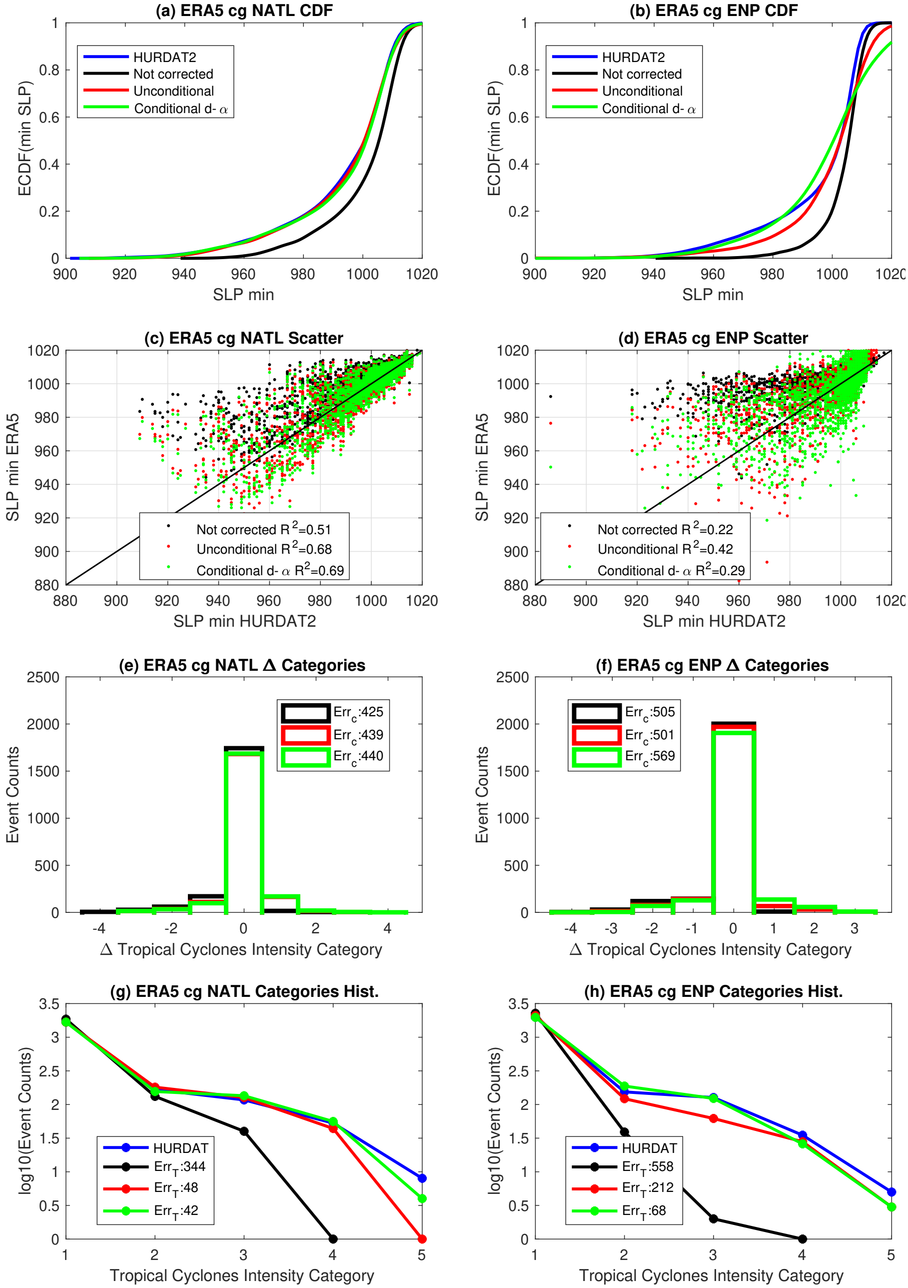

Fig. 8 As in Fig. 7 but for a realization of the ERA5 cg data sample, using $\alpha_c = 0.165$, $d_c = 19$.

of d and α values compared to ERA5 or ERA5 cg data (cf. Fig. 9a,c, and 5). These results point to a different dynamical representation of tropical cyclones in HighResMIP. The consequence is that the statistical dependencies between SLP, d and α in HighResMIP are not the same as in the reference data (ERA5 and HURDAT). Up to now, the unconditional and conditional bias correction methods applied to adjust cyclone properties were univariate. Hence, dependencies between the three variables (i.e. SLP minima, d and α) were not corrected by the unconditional approach, and only partly with the conditional one. Thus, the resulting tri-variate dependence structures were likely not appropriately represented by the corrected data. To account for this, we now also make use of a multivariate bias correction (MBC) method to adjust not only the univariate distributions but also the dependence between the three variables of interest. To do so, the "Rank Resampling for Distributions and Dependencies" (R2D2) method is applied to adjust jointly (SLP minima, d, α). R2D2 relies on an analogue-based method applied to the ranks of the time series to be corrected rather than to their "raw" values (Vrac, 2018). This MBC method can be easily designed to adjust both inter-variable, inter-site and temporal properties (Vrac and Thao, 2020) but is used only in its inter-variable configuration in the present study. Figure 9 shows the scatterplots of minimum SLP vs local dimension d and co-recurrence ratio α without (a,c) and with (b,d) R2D2 correction. The R2D2 correction retrieves SLP minima of order 920 hPa as well as extends the range of values of d and α, reproducing a pattern closer to the one observed in ERA5.

We next apply the unconditional and conditional bias-correction methodologies, as well as the R2D2 method to the HighResMIP simulations. We do not apply the R2D2 method to ERA5 because this is our reference dataset for the computation of the dynamical systems metrics. The main difference in applying the bias correction to model data rather than to reanalysis is that the correction has to be fitted and applied directly to free-running HighResMIP simulations. In such a context, cross-validation techniques for corrections evaluation have been recently heavily criticized (Maraun and Widmann, 2018) due to the influence of the model internal variability on the correction results. Hence, in the following, no separation into training and test data is performed: we correct the bulk cyclone statistics for all selected cyclones in the IPSL-CM6A-ATM-ICO-HR simulation. We first estimate the ECDFs and compute the Δ function between HighResMIP and HURDAT2 data. We then correct the full dataset using the unconditional, conditional on α, d – using the ERA5 cg values d_c and α_c – and R2D2 corrections. The results are shown in Figure 10. For the ECDFs (panels a,c), corrections obtained with or without the dynamical systems metrics improve, once again, the distribution of SLP minima. The conditional and unconditional corrections appear comparable in the NATL, but show a clear difference in the ENP. The R2D2 correction is virtually indistinguishable from HURDAT in both basins. When looking at the tropical cyclone intensities (panels b,d) we observe that the R2D2 correction of SLP minima provides a distribution of intensities which is very close to

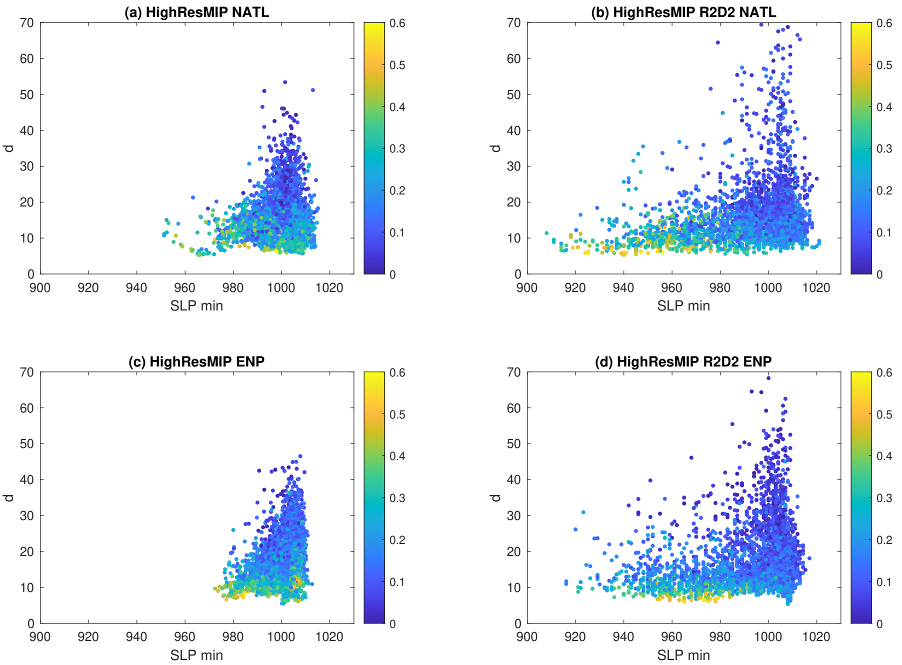

Fig. 9 Scatterplots of minimum SLP vs local dimension d and corecurrence ratio α (colorscale) calculated on uv and PV at 850 hPa for (a,c) HighResMIP; (b,d) HighResMIP corrected with R2D2, in the (a,b) North Atlantic [NATL] and (c,d) eastern North Pacific [ENP] basins.

that of the HURDAT2 data in both basins. Over the NATL, the R2D2 shows a clear improvement over the other corrections. In the ENP, it is close to the unconditional correction, which outperforms the conditional correction. Overall, these results suggest that, when applying R2D2, we are able to take into full account the information provided by the two dynamical systems metrics.

5 Summary and implications of the results

Starting from the observation that gridded datasets of tropical cyclones have a large bias in the representation of the intensity of extreme cyclones, we have introduced a bias-correction procedure. We have used: i) an unconditional quantile–quantile correction of the sea-level pressure minima of cyclones timesteps towards the HURDAT2 reference dataset; ii) a correction conditioned on two dynamical systems metrics (local dimension and co-recurrence ratio); and iii) the R2D2 correction. We have applied the first two approaches to ERA5 data, both at the highest available resolution and in a coarse-grained version. We have further applied all three approaches to data from the IPSL-CM6A-ATM-ICO-HR HighResMIP model. When using the dynamical systems metrics, we use the dynamical information from an underlying reduced phase space incorporating the square root of the horizontal kinetic

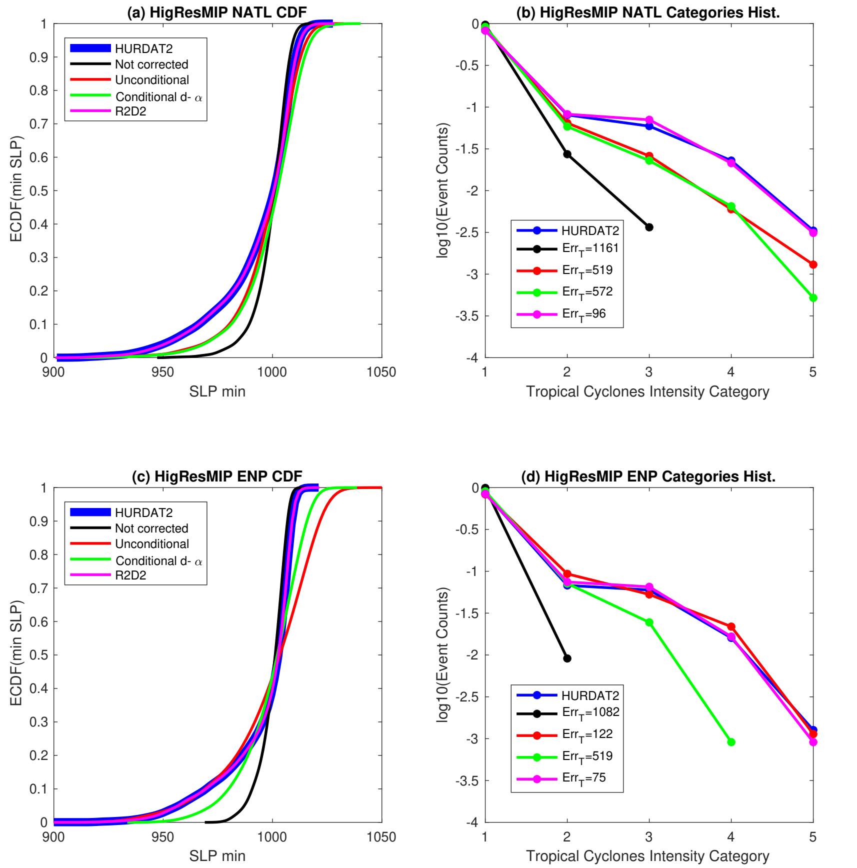

Fig. 10 Unconditional, R2D2, and conditional dynamical systems metrics bias corrections for the IPSL-CM6A-ATM-ICO-HR model. The conditional dynamical systems metrics bias corrections uses the best $d_c = 19$ and $\alpha_c = 0.165$ parameters combination from ERA5 cg. Panels (a,c) show Empirical Cumulative Density Functions (ECDFs). and (b,d) histograms of category intensities for the North Atlantic [NATL] (a,b) and eastern North Pacific [ENP] (c,d) basins.

energy uv and potential vorticity PV at 850 hPa. We have observed that the dynamical systems metrics are able to track intense cyclones as organized states of the dynamics, yielding low dimensionality and high coupling. While all bias corrections improve the bulk statistics of tropical cyclone intensity representation in our datasets, the categorisation for individual cyclones is not always improved. The conditional bias correction tends to perform better when the underlying relationship between the predictors and the response variable is strong and well-defined, whereas the unconditional bias correction can be more effective when the relationship is weaker or more variable. For the HighResMIP model, the best bias correction is the multivariate R2D2 correction which takes into account the relationships among SLP, d and α. This suggests that accounting for the multivariate dependence structures associated with the dynamical systems metrics is crucial to correcting the distribution of tropical cyclone intensities. We also observe non-neglegible differences in the bias correction performances in the two Atlantic and Pacific basins that could be further investigated in the future. For example, the conditional bias correction in the HighResMIP model underperforms in the ENP relative to its unconditional counterpart, yet this is not observed in the reanalysis. We also point out that while the optimal combination of d and α shows some variability when reshuffling the data, the changes are small. While it is true that the sample used in this study is large, with over 10000 storm timesteps, we would need to repeat the grid-search if significant changes in the storm sample occur, such as a major shift in the frequency or intensity of storms.

These considerations have a number of concrete implications for current research on tropical cyclones. Current GCMs — and even reanalysis products — struggle in reproducing minimum sea-level pressures comparable to those observed. Our study offers a way of mapping intense cyclones in d, α space and a procedure to correct biases in both century-long reanalysis products and high-resolution GCMs. This, in turn, may provide a strategy for studying changes in tropical cyclone intensity driven by anthropogenic forcing. Indeed, while d and α may not be used to provide a deterministic indication of cyclone intensity, they do provide a robust constraint for statistical correction. The large range of local dimensions associated with the dynamics of different phases of tropical cyclones may explain why it is so difficult to adequately represent them in numerical models. Follow-up studies will include the use of a larger set of HighResMIP data under different forcing scenarios, to test systematically the R2D2 correction on model data. The bias correction procedures will then be adapted to take into account the non-stationarities introduced by anthropogenic forcing, e.g. by replacing the quantile-quantile mapping with a CDF-t correction (Vrac et al, 2012) allowing to account for climate change in the correction procedure. A further avenue for future work will be to move from the pointwise correction of minimum SLP performed here, to correcting the spatial structure of the field, using multivariate bias correction techniques (e.g. Cannon, 2018; Vrac, 2018; Robin et al, 2019; Vrac and Thao, 2020) or tools from machine learning (e.g. François et al, 2021).

Statements and declarations

- Funding: the authors acknowledge the support of the INSU-CNRS-LEFE-MANU grant (project CROIRE), as well as the grant ANR-19-ERC7-0003 (BOREAS). This work has received support from the European Union's Horizon 2020 research and innovation programme (Grant agreement No. 101003469, XAIDA) and from the European Research Council (ERC) under the European Union's Horizon 2020 research and innovation programme (Grant agreement No. 948309, CENÆ project). MV was partly supported by the "COESION" project funded by the French National program LEFE

(Les Enveloppes Fluides et l'Environnement), as well as the French National "Explore2" project funded by the French Ministry of Ecological Transition (MTE) and the French Office for Biodiversity (OFB).
- Conflict of interest: The authors declare no conflict of interest.
- Ethics approval: Not applicable.
- Consent to participate: Not applicable.
- Consent for publication: Not applicable.
- Availability of data and materials: ERA5 is the latest climate reanalysis being produced by ECMWF as part of implementing the EU- funded Copernicus Climate Change Service (C3S), providing hourly data on atmospheric, land-surface and sea-state parameters together with estimates of uncertainty from 1979 to present day. ERA5 data are available on the C3S Climate Data Store on regular latitude-longitude grids at 0.25° x 0.25° resolution at https://cds.climate.copernicus.eu, accessed on 2022-04-11. The Atlantic hurricane database (HURDAT2) 1851-2020 is publicly available at https://www.nhc.noaa.gov/data/hurdat/hurdat2-1851-2020-020922.txt, accessed on 2022-04-11. The IPSL simulations are available upon request.
- Code availability: The main results of this work were obtained using Matlab. The scripts for computing the dimension and the corecurrence coefficient are available by downloading the package https://fr.mathworks.com/matlabcentral/fileexchange/95768-attractor-local-dimension-and-local-persistence-computation
- Authors' contributions: DF performed the analysis. DF and GM co-designed the analyses. ST and SB prepared the datasets. All authors participated to the manuscript preparation and contributed to the interpretation of the results.

References

Bhalachandran S, Chavas DR, Jr FDM, et al (2020) Characterizing the Energetics of Vortex-Scale and Sub-Vortex-Scale Asymmetries during Tropical Cyclone Rapid Intensity Changes. Journal of the Atmospheric Sciences 77(1):315–336. https://doi.org/10.1175/JAS-D-19-0067.1, URL https://journals.ametsoc.org/view/journals/atsc/77/1/jas-d-19-0067.1.xml, publisher: American Meteorological Society Section: Journal of the Atmospheric Sciences

Boucher O, Servonnat J, Albright AL, et al (2020) Presentation and evaluation of the ipsl-cm6a-lr climate model. Journal of Advances in Modeling Earth Systems 12(7):e2019MS002,010

Brunetti M, Kasparian J, Vérard C (2019) Co-existing climate attractors in a coupled aquaplanet. Climate Dynamics 53(9-10):6293–6308

Camargo SJ, Wing AA (2016) Tropical cyclones in climate models. WIREs Clim Change 7:211–237. https://doi.org/https://doi.org/10.1002/wcc.373

Camargo SJ, Emanuel KA, Sobel AH (2007) Use of a genesis potential index to diagnose ENSO effects on tropical cyclone genesis. Journal of Climate 20(19):4819–4834

Cannon AJ (2018) Multivariate quantile mapping bias correction: an n-dimensional probability density function transform for climate model simulations of multiple variables. Climate dynamics 50(1):31–49

Cannon AJ, Sobie SR, Murdock TQ (2015) Bias correction of gcm precipitation by quantile mapping: how well do methods preserve changes in quantiles and extremes? Journal of Climate 28(17):6938–6959

Cao L (1997) Practical method for determining the minimum embedding dimension of a scalar time series. Physica D: Nonlinear Phenomena 110(1-2):43–50

Caron LP, Jones CG, Winger K (2011) Impact of resolution and downscaling technique in simulating recent atlantic tropical cylone activity. Climate dynamics 37(5):869–892

Carstens JD, Wing AA (2020) Tropical cyclogenesis from self-aggregated convection in numerical simulations of rotating radiative-convective equilibrium. Journal of Advances in Modeling Earth Systems 12(5):e2019MS002,020

Chang EK, Guo Y (2007) Is the number of north atlantic tropical cyclones significantly underestimated prior to the availability of satellite observations? Geophysical Research Letters 34(14)

Crisanti A, Falcioni M, Vulpiani A, et al (1991) Lagrangian chaos: transport, mixing and diffusion in fluids. La Rivista del Nuovo Cimento (1978-1999) 14(12):1–80

De Luca P, Messori G, Pons FM, et al (2020) Dynamical systems theory sheds new light on compound climate extremes in europe and eastern north america. Quarterly Journal of the Royal Meteorological Society 146(729):1636–1650

Dubos T, Dubey S, Tort M, et al (2015) Dynamico-1.0, an icosahedral hydrostatic dynamical core designed for consistency and versatility. Geoscientific Model Development 8(10):3131–3150

Dunkerton TJ, Montgomery M, Wang Z (2009) Tropical cyclogenesis in a tropical wave critical layer: Easterly waves. Atmospheric Chemistry and Physics 9(15):5587–5646

Emanuel K (2021) Response of global tropical cyclone activity to increasing CO2: Results from downscaling CMIP6 models. J Climate 34:57–70. https://doi.org/10.1175/JCLI-D-20-0367.1

Emanuel KA (1986) An air-sea interaction theory for tropical cyclones. part i: Steady-state maintenance. Journal of Atmospheric Sciences 43(6):585–605

Emanuel KA (1997) Some aspects of hurricane inner-core dynamics and energetics. Journal of the Atmospheric Sciences 54:1014–1026. https://doi.org/10.1175/1520-0469(1997)054⟨1014:SAOHIC⟩2.0.CO;2

Faranda D, Messori G, Yiou P (2017) Dynamical proxies of north atlantic predictability and extremes. Scientific reports 7:41,278

Faranda D, Lembo V, Iyer M, et al (2018) Computation and characterization of local subfilter-scale energy transfers in atmospheric flows. Journal of the Atmospheric Sciences 75(7):2175–2186

Faranda D, Alvarez-Castro MC, Messori G, et al (2019) The hammam effect or how a warm ocean enhances large scale atmospheric predictability. Nature communications 10(1):1–7

Faranda D, Messori G, Yiou P (2020) Diagnosing concurrent drivers of weather extremes: application to warm and cold days in north america. Climate Dynamics 54(3):2187–2201

Faranda D, Messori G, Yiou P, et al (2023) Dynamical footprints of hurricanes in the tropical dynamics. Chaos: An Interdisciplinary Journal of Nonlinear Science 33(1):013,101

François B, Thao S, Vrac M (2021) Adjusting spatial dependence of climate model outputs with cycle-consistent adversarial networks. Climate Dynamics 57(11):3323–3353

Freitas ACM, Freitas JM, Todd M (2010) Hitting time statistics and extreme value theory. Probability Theory and Related Fields 147(3-4):675–710

Fu B, Peng MS, Li T, et al (2012) Developing versus nondeveloping disturbances for tropical cyclone formation. part ii: Western north pacific. Monthly weather review 140(4):1067–1080

Grinsted A, Ditlevsen P, Christensen JH (2019) Normalized us hurricane damage estimates using area of total destruction, 1900- 2018. Proceedings of the National Academy of Sciences 116(48):23,942–23,946

Gualandi A, Avouac JP, Michel S, et al (2020) The predictable chaos of slow earthquakes. Science advances 6(27):eaaz5548

Haarsma RJ, Roberts MJ, Vidale PL, et al (2016) High resolution model intercomparison project (HighResMIP v1. 0) for CMIP6. Geoscientific Model Development 9(11):4185–4208

Hersbach H, Bell B, Berrisford P, et al (2020) The era5 global reanalysis. Quarterly Journal of the Royal Meteorological Society 146(730):1999–2049

Hochman A, Alpert P, Harpaz T, et al (2019) A new dynamical systems perspective on atmospheric predictability: Eastern mediterranean weather regimes as a case study. Science advances 5(6):eaau0936

Hochman A, Messori G, Quinting JF, et al (2021a) Do atlantic-european weather regimes physically exist? Geophysical Research Letters 48(20):e2021GL095,574

Hochman A, Scher S, Quinting J, et al (2021b) A new view of heat wave dynamics and predictability over the eastern mediterranean. Earth System Dynamics 12(1):133–149

Hourdin F, Rio C, Grandpeix JY, et al (2020) Lmdz6a: The atmospheric component of the ipsl climate model with improved and better tuned physics. Journal of Advances in Modeling Earth Systems 12(7):e2019MS001,892

Kim D, Moon Y, Camargo SJ, et al (2018) Process-oriented diagnosis of tropical cyclones in high-resolution gcms. Journal of Climate 31(5):1685–1702

Klotzbach PJ, Bell MM, Bowen SG, et al (2020) Surface pressure a more skillful predictor of normalized hurricane damage than maximum sustained wind. Bulletin of the American Meteorological Society 101(6):E830–E846

Knaff JA, Sampson CR, Kucas ME, et al (2021) Estimating tropical cyclone surface winds: Current status, emerging technologies, historical evolution, and a look to the future. Tropical Cyclone Research and Review 10:125–150. https://doi.org/https://doi.org/10.1016/j.tcrr.2021.09.002

Knutson T, Camargo SJ, Chan JCL, et al (2019) Tropical cyclones and climate change assessment: Part I: Detection and Attribution. Bull Amer Meteor Soc 100:1987–2007. https://doi.org/10.1175/BAMS-D-18-0189.1

Knutson T, Camargo SJ, Chan JC, et al (2020) Tropical cyclones and climate change assessment: Part ii: Projected response to anthropogenic warming. Bulletin of the American Meteorological Society 101(3):E303–E322

Krishnamurti T, Pattnaik S, Stefanova L, et al (2005) The hurricane intensity issue. Monthly weather review 133(7):1886–1912

Landsea CW, Franklin JL (2013) Atlantic hurricane database uncertainty and presentation of a new database format. Monthly Weather Review 141(10):3576–3592

Lee CY, Camargo SJ, Sobel AH, et al (2020) Statistical–dynamical downscaling projections of tropical cyclone activity in a warming climate: Two diverging genesis scenarios. J Climate 33:4815–4834. https://doi.org/10.1175/JCLI-D-19-0452.1

Levich E, Tzvetkov E (1985) Helical inverse cascade in three-dimensional turbulence as a fundamental dominant mechanism in mesoscale atmospheric phenomena. Physics reports 128(1):1–37

Li H, Sheffield J, Wood EF (2010) Bias correction of monthly precipitation and temperature fields from intergovernmental panel on climate change ar4 models using equidistant quantile matching. Journal of Geophysical Research: Atmospheres 115(D10)

Lorenz EN (1990) Can chaos and intransitivity lead to interannual variability? Tellus A 42(3):378–389

Lucarini V, Faranda D, Wouters J (2012) Universal behaviour of extreme value statistics for selected observables of dynamical systems. Journal of statistical physics 147(1):63–73

Lucarini V, Faranda D, de Freitas JMM, et al (2016) Extremes and recurrence in dynamical systems. John Wiley & Sons

Manganello JV, Hodges KI, Kinter III JL, et al (2012) Tropical cyclone climatology in a 10-km global atmospheric gcm: toward weather-resolving climate modeling. Journal of Climate 25(11):3867–3893

Maraun D (2016) Bias correcting climate change simulations-a critical review. Current Climate Change Reports 2(4):211–220

Maraun D, Widmann M (2018) Cross-validation of bias-corrected climate simulations is misleading. Hydrology and Earth System Sciences 22(9):4867–4873. https://doi.org/10.5194/hess-22-4867-2018, URL https://hess.copernicus.org/articles/22/4867/2018/

Messori G, Faranda D (2021) Characterising and comparing different palaeoclimates with dynamical systems theory. Climate of the Past 17(1):545–563

Messori G, Caballero R, Faranda D (2017) A dynamical systems approach to studying midlatitude weather extremes. Geophysical Research Letters 44(7):3346–3354

Messori G, Harnik N, Madonna E, et al (2021) A dynamical systems characterization of atmospheric jet regimes. Earth System Dynamics 12(1):233–251

Michelangeli PA, Vrac M, Loukos H (2009) Probabilistic downscaling approaches: Application to wind cumulative distribution functions. Geophysical Research Letters 36(11)

Montgomery MT, Smith RK (2017) Recent developments in the fluid dynamics of tropical cyclones. Annual Review of Fluid Mechanics 49:541–574

Moon Y, Kim D, Camargo SJ, et al (2020) Azimuthally averaged wind and thermodynamic structures of tropical cyclones in global climate models and their sensitivity to horizontal resolution. J Climate 33:1575 – 1595. https://doi.org/10.1175/JCLI-D-19-0172.1

Muller CJ, Romps DM (2018) Acceleration of tropical cyclogenesis by self-aggregation feedbacks. Proceedings of the National Academy of Sciences 115(12):2930–2935

Murakami H, Wang Y, Yoshimura H, et al (2012) Future changes in tropical cyclone activity projected by the new high-resolution mri-agcm. Journal of Climate 25(9):3237–3260

Peng MS, Fu B, Li T, et al (2012) Developing versus nondeveloping disturbances for tropical cyclone formation. part i: North atlantic. Monthly weather review 140(4):1047–1066

Roberts MJ, Camp J, Seddon J, et al (2020a) Impact of model resolution on tropical cyclone simulation using the highresmip–primavera multimodel ensemble. Journal of Climate 33(7):2557–2583

Roberts MJ, Camp J, Seddon J, et al (2020b) Projected future changes in tropical cyclones using the CMIP6 HighResMIP multimodel ensemble. Geophysical Research Letters 47(14):e2020GL088,662

Robin Y, Vrac M, Naveau P, et al (2019) Multivariate stochastic bias corrections with optimal transport. Hydrology and Earth System Sciences 23(2):773–786

Rotunno R, Chen Y, Wang W, et al (2009) Large-eddy simulation of an idealized tropical cyclone. Bull Amer Meteor Soc 90:1783–1788. https://doi.org/10.1175/2009BAMS2884.1

Schubert S, Lucarini V (2015) Covariant lyapunov vectors of a quasi-geostrophic baroclinic model: analysis of instabilities and feedbacks. Quarterly Journal of the Royal Meteorological Society 141(693):3040–3055

Simpson RH, Saffir H (1974) The hurricane disaster potential scale. Weatherwise 27(8):169

Smith AB, Katz RW (2013) Us billion-dollar weather and climate disasters: data sources, trends, accuracy and biases. Natural hazards 67(2):387–410

Sugi M, Murakami H, Yoshida K (2017) Projection of future changes in the frequency of intense tropical cyclones. Climate Dynamics 49:619–632

Tang J, Byrne D, Zhang JA, et al (2015) Horizontal transition of turbulent cascade in the near-surface layer of tropical cyclones. Journal of the Atmospheric Sciences 72(12):4915–4925

Ullrich PA, Zarzycki CM, McClenny EE, et al (2021) Tempestextremes v2. 1: a community framework for feature detection, tracking and analysis in large datasets. Geoscientific Model Development Discussions pp 1–37

Vrac M (2018) Multivariate bias adjustment of high-dimensional climate simulations: the rank resampling for distributions and dependences (r 2 d 2) bias correction. Hydrology and Earth System Sciences 22(6):3175–3196

Vrac M, Thao S (2020) R 2 d 2 v2. 0: accounting for temporal dependences in multivariate bias correction via analogue rank resampling. Geoscientific Model Development 13(11):5367–5387

Vrac M, Drobinski P, Merlo A, et al (2012) Dynamical and statistical downscaling of the french mediterranean climate: uncertainty assessment. Natural Hazards and Earth System Sciences 12(9):2769–2784

Vulpiani A (2010) Chaos: from simple models to complex systems, vol 17. World Scientific

Wolf A, Swift JB, Swinney HL, et al (1985) Determining lyapunov exponents from a time series. Physica D: Nonlinear Phenomena 16(3):285–317

Yoshida K, Sugi M, Mizuta R, et al (2017) Future changes in tropical cyclone activity in high-resolution large-ensemble simulations. Geophysical Research Letters 44(19):9910–9917

Zhao M, Held IM (2010) An analysis of the effect of global warming on the intensity of atlantic hurricanes using a gcm with statistical refinement. Journal of Climate 23(23):6382–6393